THE JOURNAL OF BIOLOGICAL CHEMISTRY VOL. 288, NO. 15, pp. 10513–10521, April 12, 2013

Oligomeric Structure and Functional Characterization of *Caenorhabditis elegans* Innexin-6 Gap Junction Protein*[S]

Received for publication, October 16, 2012, and in revised form, March 1, 2013 Published, JBC Papers in Press, March 4, 2013, DOI 10.1074/jbc.M112.428383

Atsunori Oshima[‡§1], **Tomohiro Matsuzawa**[¶], **Kouki Nishikawa**[‡], **and Yoshinori Fujiyoshi**[‡§]

From the [‡]*Cellular and Structural Physiology Institute (CeSPI), Nagoya University, Furo-cho, Chikusa-ku, Nagoya 464-8601, the* [§]*Department of Basic Medicinal Sciences, Graduate School of Pharmaceutical Sciences, Nagoya University, Furo-cho, Chikusa-ku, Nagoya 464-8601, and the* [¶]*Department of Biophysics, Graduate School of Science, Kyoto University, Oiwake, Kitashirakawa, Sakyo-ku, Kyoto 606-8502*

Background: Invertebrates possess gap junction channels composed of innexins.
Results: The molecular dimension, oligomeric state, and permeability of *C. elegans* INX-6 channels were determined by structural, biochemical, and functional studies.
Conclusion: INX-6 channels have a larger overall structure and higher permeability as compared with connexins.
Significance: Innexin channels appear to be distinct from connexin channels in terms of structure and function.

Innexin is the molecular component of invertebrate gap junctions. Here we successfully expressed and purified *Caenorhabditis elegans* innexin-6 (INX-6) gap junction channels and characterized the molecular dimensions and channel permeability using electron microscopy (EM) and microinjection of fluorescent dye tracers, respectively. Negative staining and thin-section EM of isolated INX-6 gap junction membranes revealed a loosely packed hexagonal lattice and a greater cross-sectional width than that of connexin26 and connexin43 (Cx43)-GFP. In gel filtration analysis, the elution profile of purified INX-6 channels in dodecyl maltoside solution exhibited a peak at ~400 kDa that was shifted to ~800 kDa in octyl glucose neopentyl glycol. We also obtained the class averages of purified INX-6 channels from these peak fractions by single particle analysis. The class average from the ~800-kDa fraction showed features of the junction form with a longitudinal height of 220 Å, a channel diameter of 110 Å in the absence of detergent micelles, and an extracellular gap space of 60 Å, whereas the class averages from the ~400-kDa fraction showed diameters of up to 140 Å in the presence of detergent micelles. These findings indicate that the purified INX-6 channels are predominantly hemichannels in dodecyl maltoside and docked junction channels in octyl glucose neopentyl glycol. Dye transfer experiments revealed that the INX-6-GFP-His channels are permeable to 3- and 10-kDa tracers, whereas no significant amounts of these tracers passed through the Cx43-GFP channels. Based on these findings, INX-6 channels have a larger overall structure and greater permeability than connexin channels.

Intercellular communication is directly mediated via gap junction channels, which generally transport small molecules up to 1–2 kDa (1), making them essential for metabolic homeostasis, pattern formation during embryo development, synchronization of heart muscle contraction, and signal transmission in electrical synapses (2, 3). Gap junction channels comprise face-to-face docked single membrane channels (hemichannels) that form a hexagonal array in the native tissues (4, 5).

Connexin is the molecular component of vertebrate gap junctions, and the connexin family includes more than 20 isoforms identified from mammals, chicks, amphibians, and fish (6). Invertebrates possess an evolutionarily distinct molecule, innexin, which is thought to have a similar topology to connexin, *i.e.* four transmembrane helices, two extracellular loops, and N and C termini located on the cytoplasmic side (7). Innexin was originally identified from *Drosophila* and *Caenorhabditis elegans* mutants exhibiting anomalous coupling between neurons and muscles by conventional genetic methods (8–10) and confirmed to form intercellular channels by electrical coupling of paired *Xenopus* oocytes (11). The innexin gene family is quite large; *e.g.* there are 8 innexins in fly, 25 innexins in worm, and 21 innexins in leech (12, 13). Innexin homologs identified in vertebrates are termed pannexins (14). Pannexin channels are thought to function as single membrane channels *in vivo*, *e.g.* to release ATP working cooperatively with purinergic receptors for T-cell activation at the immune synapse or for recruiting phagocytes during apoptosis (15, 16).

Expression patterns of all 25 innexins in *C. elegans* analyzed by GFP under the control of entire promoter regions exhibit an overlapping and complementary distribution of a variety of innexins in complex tissues (17). *C. elegans* innexin-6 (*inx-6*, INX-6)[2] is expressed in pharyngeal tissues. It is first expressed during embryogenesis in cells likely to be pharyngeal precursors and then in the corpus muscles and isthmus marginal cells of the pharynx throughout the larval and adult stages (18). *inx-6*

* This work was supported by grants-in-aid for scientific research (S) (to Y. F.), the Platform for Drug Design, Discovery and Development (to A. O.) from the Ministry of Education, Culture, Sports, Science and Technology (MEXT), Japan, and the Japan New Energy and Industrial Technology Development Organization (NEDO) (to Y. F.).
[S] This article contains supplemental Fig. 1.
[1] To whom correspondence should be addressed. Tel.: 81-52-747-6794; Fax: 81-52-747-6795; E-mail: atsu@cespi.nagoya-u.ac.jp.

[2] The abbreviations used are: INX, innexin; Cx, connexin; DDM, *n*-dodecyl-β-D-maltopyranoside, dodecyl maltoside; OGNG, octyl glucose neopentyl glycol; SR101, sulforhodamine 101; TR, Texas Red; 3k-TR, 3-kDa Texas Red dextran; 10k-TR, 10-kDa Texas Red dextran; 70k-TR, 70-kDa Texas Red dextran.

is a temperature-sensitive allele, and *inx-6* mutants exhibit feeding deficits as pharyngeal muscle contraction is unsynchronized and the anterior pharyngeal muscles are less electrically coupled than the posterior metacorpus muscles. Expression of *inx-6* in the metacorpus overlaps with *eat-5*, but the two genes are not fully interchangeable, suggesting that *inx-6* and *eat-5* serve similar but not identical functions *in vivo* (18).

Structural studies of connexin gap junction channels were recently performed using electron crystallography and x-ray crystallography (19–21). Knowledge of the three-dimensional structure of innexin channels, however, is very limited because neither high-resolution images nor purification of recombinant innexin channels have been reported. EM observation of invertebrate gap junctions was performed before molecular cloning of innexin genes. In freeze fracture or negatively stained images, gap junctions in crayfish appear similar to those of vertebrates, but the hexagonal arrays of the channels often exhibit swollen packing with a unit cell of up to ~200 Å (22). Studies using electron tomography estimated both the periodicity of the channels and the extracellular gap size between the junction membranes isolated from the lateral giant fibers of crayfish (23). Although the native gap junctions in *C. elegans* have been observed by thin-section EM (24, 25), the molecular structure of innexin channels remains poorly resolved.

To further elucidate the structure of innexin gap junction channels, we isolated and characterized recombinant *C. elegans* INX-6 channels. INX-6 channels were overexpressed in Sf9 cells, and EM observation revealed the isolated gap junction plaques of INX-6. Negative staining and thin-section EM imaging methods were used to evaluate the channel distance and the width of the gap junction membranes. INX-6-GFP-His channels, in which the GFP-His tag was fused at the C terminus of INX-6, were solubilized and purified in dodecyl maltoside (DDM) detergent solution and then analyzed by gel filtration with different detergents in running buffer. Single particle analysis was performed to determine the oligomeric state and molecular dimensions of purified INX-6 channels. We also performed a dye transfer assay with various sizes of tracers, sulforhodamine 101 (SR101, 607 Da), 3-kDa Texas Red dextran (3k-TR), 10-kDa Texas Red dextran (10k-TR), and 70-kDa Texas Red dextran (70k-TR). Our results indicate that INX-6 forms similar but distinct gap junction channels from connexins in terms of the molecular dimensions and permeability. These findings are consistent with the notion that invertebrates possess a wide limiting pore diameter as compared with vertebrates (26).

EXPERIMENTAL PROCEDURES

Expression and Purification of Recombinant INX-6 Gap Junction Channels—The gene coding the full-length *C. elegans* INX-6 was cloned into pFastBac1 (Invitrogen) for expression in Sf9 cells. A His tag (His_6) or GFP-His tag (GFP plus His_8) was inserted along with a thrombin cleavage recognition sequence at the C terminus of INX-6 and then cloned into pFastBac1. Recombinant baculoviruses of INX-6, INX-6-His, or INX-6-GFP-His were generated from recombinant bacmids and used to infect Sf9 cells at 27 °C. After infection for 30 h, the cells were harvested by low speed centrifugation followed by freezing in liquid nitrogen and storage at −80 °C. For membrane preparation, cells were suspended in buffer containing 10 mM Tris (pH 7.5), 150 mM NaCl, and 1 mM phenylmethylsulfonyl fluoride and disrupted by sonication for 90 s. The cell suspension was centrifuged at 22,100 × *g* for 25 min. The collected INX-6-His or INX-6-GFP-His membranes were resuspended and solubilized in buffer containing 10 mM Tris (pH 7.5), 150 mM NaCl, and 1% DDM for 30 min. The debris was discarded by centrifugation at 21,300 × *g* for 10 min. The supernatant was bound to the nickel-nitrilotriacetic acid-agarose (Qiagen), washed with 10 mM L-histidine, and eluted with 300 mM L-histidine. Isolated membranes and purified channels were checked by SDS-PAGE and Western blot with anti-His antibody (Qiagen). All membrane preparation and purification steps were conducted at 4 °C. The human Cx26 channel preparation protocol was described previously (27).

Expression and Isolation of Cx43-GFP Gap Junction Channels—Human Cx43 was fused by the C-terminal GFP tag and cloned into pTRE3G (Clontech). Cx43-GFP was stably expressed using the Tet-On® 3G inducible expression system (Clontech). After cloning the Cx43-GFP-positive HeLa cells, the cells were grown in 500-cm^2 dishes in tetracycline (Tet)-free Dulbecco's modified Eagle's medium supplemented with 10% Tet system approved FBS (Clontech) and 1% penicillin/streptomycin (Gibco) at 37 °C. Cx43-GFP gene expression was induced by 1 μg/ml doxycycline and 4.5 μM trichostatin A (Sigma) at 90–95% confluency, and the cells were harvested 48–54 h after induction. Cx43-GFP junction membranes were isolated as described previously (28) without dialysis. Briefly, Cx43-GFP-induced HeLa cells were resuspended in HEPES buffer (10 mM HEPES, pH 7.5, 0.8% NaCl) and dispersed by short term sonication. Cx43-GFP membranes were enriched by ultracentrifugation on a sucrose gradient. The materials at the 35%/49% interface were further extracted by adding 2.8% Tween 20 and 13 mg/ml 1,2-diheptanoyl-*sn*-phosphatidylcholine. After ultracentrifugation, the Cx43-GFP membranes were resuspended in HEPES buffer.

Electron Microscopy for Negative Staining and Thin-section Imaging—All images were recorded on a JEOL 1010 with 40,000× magnification operated at 100 kV. The specimens were negatively stained with 2% uranyl acetate. For cross-sectional images, we used the conventional ultrathin sectioning method. Briefly, the pelleted membranes were fixed in 2% glutaraldehyde followed by a second fixation with 2% OsO_4 at 4 °C. The specimen was subsequently stained with 1% uranyl acetate, embedded in epoxy resin, and allowed to harden at 60 °C overnight. The ultrathin sections were 70–80 nm thick. Negative stain images (see Figs. 3, *A*–C, and 4, *C* and *E*) were obtained using a 2K slow scan charge-coupled device camera (Gatan, 24-μm pixel size) with an image pixel size of 0.57 nm. Thin-section images were obtained with a 2K complementary metal oxide semiconductor TemCam-F216 (Tietz, 15.6-μm pixel size) with 0.22 nm/pixel. For single particle analysis, all data were obtained with a 4K complementary metal oxide semiconductor TemCam-F416 (Tietz, 15.6-μm pixel size) with an image pixel size of 0.286 nm.

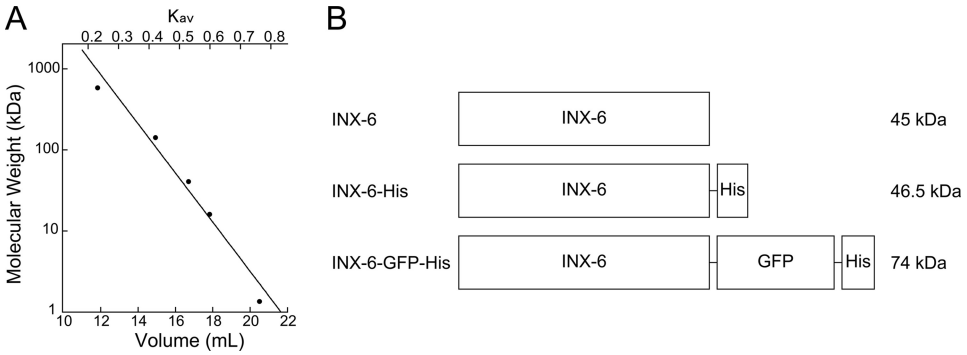

FIGURE 1. **Calibration of gel filtration column and INX-6 gene constructs.** *A*, calibration plot for gel filtration analysis using a Superose 6 column. The protein markers thyroglobulin (670 kDa), γ-globulin (158 kDa), ovalbumin (44 kDa), myoglobin (17 kDa), and vitamin B12 (1.35 kDa), are plotted as *filled circles*. The partition coefficient K_{av} is defined as, $K_{av} = (V_e - V_o)/(V_b - V_o)$, where V_e is the elution volume, V_o is the void volume defined as 7.4 ml by blue dextran 2000 (2000 kDa), and V_b is the total volume of column beads. The apparent molecular masses of INX-6 are calculated based on the relationship between K_{av} and the log of the molecular mass (*solid line*). *B*, schematic representations of INX-6 gene constructs in this study. Indicated gene boxes represent only relative size. All C-terminal tags were designed to be removed by thrombin. Molecular masses are shown on the *right*.

Size Exclusion Chromatography and Single Particle Analysis of Purified INX-6 Channels—After digesting the GFP-His tag with thrombin, INX-6 proteins were loaded onto a Superose 6 10/300 GL column (GE Healthcare) equilibrated in 10 mM Tris (pH 7.5), 300 mM NaCl, 1 mM dithiothreitol, and 0.05% DDM. The purified INX-6 channels were also analyzed in 0.1% octyl glucose neopentyl glycol (OGNG) in gel filtration buffer to further study the oligomeric form. The column was calibrated with molecular mass standards (thyroglobulin, 670 kDa; γ-globulin, 158 kDa; ovalbumin, 44 kDa; myoglobin, 17 kDa; and vitamin B12, 1.35 kDa, see Fig. 1*A*) and run at a flow rate of 0.5 ml/min. Fractions around the highest peak of UV 280 nm absorbance were analyzed by SDS-PAGE and native PAGE. The protein bands were visualized using Coomassie Brilliant Blue-R250 or SimplyBlue SafeStain (Invitrogen). Single particle analysis was performed using the negative stain EM images of purified INX-6 channels taken from gel filtration fractions at ~800 kDa and at ~400 kDa. Picked particles were aligned and classified based on multivariate statistical analysis by EMAN (29). Total numbers of picked particles were 2728 for the junction channel and 7283 for the hemichannel.

Microinjection of Fluorescent Tracers—INX-6-GFP-His recombinant viruses were infected to the attached Sf9 cells in 35-mm glass bottom dishes. After infection for 24 h, fluorescent tracers were injected into the cells forming the gap junction plaque signals. Recombinant viruses expressing intact GFP were used as negative controls of the Sf9 cells. For Cx43-GFP, stable HeLa cells were cultured in 35-mm glass bottom dishes. The tracers were injected 24 h after induction by doxycycline and trichostatin A. Mock-transfected cells were stable HeLa cells with no induction of Cx43-GFP expression and were used as negative controls. Dye transfer was captured on a fluorescent microscope IX81 (Olympus) 1 min after injection. One set was defined as 10–15 injections. *n* indicates the number of sets. The fluorescent tracers, SR101 (607 Da), 3k-TR, 10k-TR, and 70k-TR, were purchased from Molecular Probes. As for the Texas Red tracers, conjugated dextran has a molecular mass distribution range as follows: 3-kDa, 1500–3000 Da; 10-kDa, 9000–11,000 Da; and 70-kDa, 60,000–90,000 Da.

RESULTS

INX-6 constructs with different C-terminal tags were generated in accordance with the experimental aim. The intact INX-6 construct was used for the negative stain EM observation of gap junction plaques and for thin-section imaging. For purification, either a His tag or a GFP-His tag was fused to INX-6 (INX-6-His, INX-6-GFP-His), and the GFP-His tag was digested by thrombin before loading proteins on a gel filtration column. INX-6-GFP-His was also used for the dye transfer assay. These constructs are summarized in Fig. 1*B*.

Expression and Purification of His-tagged INX-6 Gap Junction Channels—INX-6-His gap junction membranes were isolated from Sf9 cells by sonication and one-step centrifugation. This isolation protocol yielded poorer purity of innexin proteins than the alkali preparation for connexin gap junction membranes (Fig. 2, *lane 1*) (30). INX-6-His protein expression in the membrane fraction, however, was detected by Western blot with the anti-His antibody (Fig. 2, *lane 3*). The signal appeared at ~37 kDa, which is smaller than that estimated from the amino acid sequence, 45 kDa. This might be due to the globular form and/or charge distribution, which is specific to denatured INX-6 peptides in SDS buffer. After solubilization and purification with nickel-nitrilotriacetic acid agarose in DDM solution, the INX-6-His band clearly appeared on the Coomassie Brilliant Blue-stained gel (Fig. 2, *lane 2*), consistent with the signal detected by the anti-His antibody (Fig. 2, *lane 4*).

INX-6 Forms Loosely Packed Hexagonal Gap Junction Plaques in Sf9 Cells—Gap junction plaques of INX-6 in isolated membrane fractions observed by negative stain EM very clearly showed the channel pores (Fig. 3*A*). The contribution of endogenous innexin expression to the formation of recombinant INX-6 gap junctions, if any, was thought to be negligible as no gap junction plaque was observed in control Sf9 cells (data not shown). Fast Fourier transform from the selected area of INX-6 plaques resulted in blurred hexagonal diffraction spots (Fig. 3*D*), suggesting that the INX-6 channels form a loosely packed array but have packing similar to the gap junction plaques of Cx26 in Sf9 cells and Cx43-GFP in HeLa cells (Fig. 3, *B*, *C*, *E*, and *F*). We estimated the channel distances using the fast Fourier

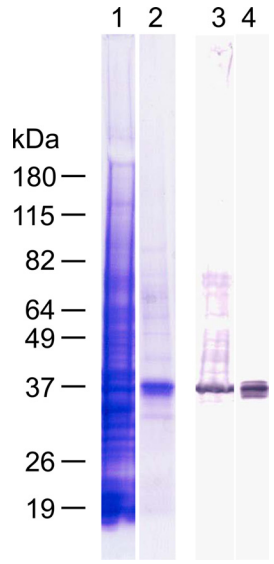

FIGURE 2. **SDS-PAGE and Western blots of INX-6-His channels.** The Coomassie Brilliant Blue-stained gel (*lanes 1* and *2*) and corresponding Western blots probed with anti-His antibody (*lanes 3* and *4*) are shown. Isolated membranes (*lanes 1* and *3*) and eluate from nickel-nitrilotriacetic acid chromatography (*lanes 2* and *4*) of INX-6-His channels were loaded on the gel. The molecular mass markers are on the *left*. Western blot signals correspond to the 37-kDa band in Coomassie Brilliant Blue staining, which confirmed that the 37-kDa protein was INX-6.

transform diffraction spots from several selected images of INX-6 gap junction plaques. Assuming a hexagonal lattice, the adjacent INX-6 channels were aligned with a pitch of as much as 110.1 ± 3.3 Å (n = 8) (Table 1). The channel distance of INX-6 varied depending on the selected plaques but was never less than 100 Å. Gap junction plaques of Cx26 and Cx43-GFP in our preparation revealed a channel pitch of 93.9 ± 1.1 Å (n = 11) and 77.2 ± 1.1 Å (n = 9), respectively (Table 1), consistent with the cell parameters of vertebrate gap junctions, between 75 and 95 Å (31–39).

We subsequently performed thin-section EM of isolated INX-6 gap junction plaques to measure the cross-sectional width (Fig. 3, *G*, *H*, and *I*). The width of INX-6 gap junctions was 184.1 ± 4.3 Å (n = 12) as compared with 139.6 ± 3.3 Å (n = 10) for Cx26 gap junctions and 162.1 ± 3.1 Å (n = 11) for Cx43-GFP junctions (Table 1). The two extracellular loops of INX-6 are thought to be longer, *i.e.* ~50 amino acids for innexins, estimated from the alignment of innexin sequences (supplemental Fig. 1), and ~30 amino acids for connexins, based on the Cx26 x-ray structure (20). The greater width of INX-6 gap junction plaques may be due to greater spacing between adjacent membranes.

Oligomeric State and Molecular Dimension of Purified INX-6 Channels—INX-6-GFP-His channels were solubilized in DDM solution and purified using nickel affinity chromatography. After thrombin digestion of the GFP-His tag, the channels were analyzed by gel filtration. The highest elution peak of UV 280 nm absorbance appeared at ~400 kDa (386 ± 8 kDa, n = 13) (Fig. 4*A*) and was confirmed to be INX-6 peptides by SDS-PAGE (Fig. 4*B*). The peak fraction was collected and subjected to negative stain EM observation. The oligomeric INX-6 channels showed homogeneous particles, some of which were oriented with their pores perpendicular to the carbon support film forming a doughnut shape (Fig. 4*C*). When nickel affinity-purified INX-6 channels were loaded in 0.1% OGNG, the absorbance of INX-6 peaked at ~800 kDa (783 ± 42 kDa, n = 7) (Fig. 4*D*). Accordingly, EM observation of the fraction at ~800 kDa in OGNG revealed many double-barreled particles (Fig. 4*E*, *square brackets*), indicating dimerization of the channels in Fig. 4*C*. In native PAGE analysis of peak fractions, we observed a major band shift of INX-6 from ~480 kDa in DDM (Fig. 4*F*, *lane 1*) to over 720 kDa in OGNG (Fig. 4*F*, *lane 2*), consistent with the UV 280 nm absorbance profiles and negative stain EM observations.

We further performed single particle analysis using the negative stain EM images. In the class averages of INX-6 channels at ~800 kDa, we found projection structures that clearly showed the typical features of docked junction channels as a side view with two detergent belts corresponding to the transmembrane region where the stain does not penetrate (Fig. 4*G*). The dimensions of the INX-6 junction structure were estimated from a representative average (Fig. 4*H*, *left*). The longitudinal height of the junction channel was 220 Å, the extracellular gap space was 60 Å, and the cytoplasmic protrusions were 45 Å wide. Because the transmembrane region, which is 140 Å in diameter, includes detergent micelles, diameters of 110 Å at the cytoplasmic and extracellular ends, where no detergent micelles are thought to contribute, may be close to the actual channel diameter. These measurements demonstrate that the molecular dimensions of the INX-6 junction channel are 1.2–1.5 times greater than those of the Cx26 channels (Fig. 4*H*, *right*) (20). This finding is consistent with the extended channel pitch and cross-sectional width of INX-6 gap junction membranes as compared with the connexins (Fig. 3 and Table 1). On the other hand, the class averages from the ~400-kDa fraction revealed that smaller size particles assumed a variety of orientations (Fig. 4*I*). A representative class average that clearly shows a channel pore in a top view has a channel diameter of ~140 Å (Fig. 4*J*), and the diameters of other class averages are similar (Fig. 4*I*). These particles are too small for junction forms, as shown in Fig. 4*H* (*left*). Based on these findings, we concluded that INX-6 channels at ~400 kDa are predominantly hemichannels, whereas the fraction at ~800 kDa includes more docked junction channels.

Dye Transfer Analysis of INX-6 Channels—INX-6-GFP-His expressed in Sf9 cells formed gap junction plaques between neighboring cells (Fig. 5*A*, *top row*, *yellow arrowheads*) but did not form junction plaques in mammalian cells (data not shown). Recombinant viruses expressing soluble GFP were generated as negative controls (Fig. 5*A*, *bottom row*). To compare the permeability with that of connexin channels, we selected Cx43-GFP as a representative connexin because Cx43 is thought to have a relatively larger limiting pore diameter and less charge selectivity than other connexin family isoforms (40). Cx43-GFP formed gap junction signals in HeLa cells (Fig. 5*B*, *top row*, *yellow arrowhead*), but not in Sf9 cells (data not shown). HeLa cells without Cx43-GFP expression were used as negative controls (Fig. 5*B*, *bottom row*). Both INX-6-GFP-His and Cx43-GFP exhibited significant transfer of SR101 within 1 min after injection (Fig. 5, *A* and *B*, *top rows*, *right panels*).

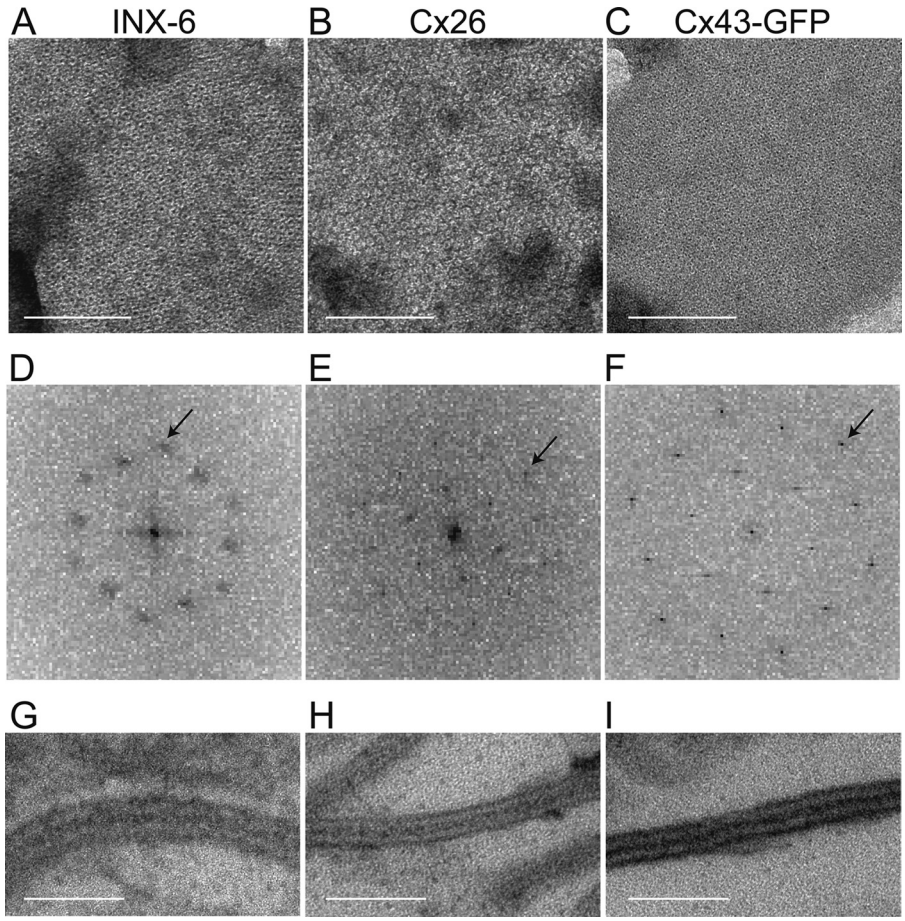

FIGURE 3. **EM observation of INX-6 and connexin gap junction channels using negative stain and thin-section imaging.** *A–C*, representative electron micrographs of isolated gap junction plaques for INX-6 (*A*), Cx26 (*B*) from Sf9 cells, and Cx43-GFP (*C*) from HeLa cells. *Bar* = 100 nm. *D–F*, fast Fourier transform diffraction spots of selected areas of gap junction plaques shown in *A–C* suggest hexagonal packing of the channels in all three constructs. *Blurred spots* indicate loosely packed INX-6 channels. *Black arrows* represent a resolution of 49 Å for INX-6 (*D*), 43 Å for Cx26 (*E*), and 32 Å for Cx43-GFP (*F*). *G–I*, ultrathin section electron micrographs of isolated gap junction membranes for INX-6 (*G*), Cx26 (*H*) from Sf9 cells, and Cx43-GFP (*I*) from HeLa cells. *Bar* = 50 nm.

TABLE 1

Estimation of channel distance and junction membrane width based on EM observation

Junction width was evaluated with edge-to-edge spacing of pixels on thin-section images.

	Channel distance	Junction membrane width
INX-6	110.1 ± 3.3 Å (n = 8)	184.1 ± 4.3 Å (n = 12)
Cx26	93.9 ± 1.1 Å (n = 11)	139.6 ± 3.3 Å (n = 10)
Cx43-GFP	77.2 ± 1.1 Å (n = 9)	162.1 ± 3.1 Å (n = 11)

To investigate the permeability of INX-6-GFP-His and Cx43-GFP, several tracers with different sizes, SR101 (607 Da), 3k-TR (3 kDa), 10k-TR (10 kDa), and 70k-TR (70 kDa), were examined. The proportion of dye-coupled cells through INX-6-GFP-His junctions was 82.7% for SR101, 46.7% for 3k-TR, and 11.6% for 10k-TR, and the transfer of 70k-TR was as high as the background (Fig. 5*C*). For Cx43-GFP channels, only SR101 transferred through more than 90% of the junctions, but the other larger dyes were not significantly different from background (Fig. 5*D*). These findings are consistent with the general criteria that gap junctions in vertebrates allow for the passage of molecules up to 1 kDa in size (1). These results indicate that, as compared with Cx43-GFP channels, INX-6 channels allow for the passage of larger molecules.

DISCUSSION

The innexin family includes a large number of family members identified in Arthropoda, Nematoda, Annelida, and ichnovirus (12). Although recent molecular studies of innexins using electrophysiology demonstrated the helical nature of the first transmembrane domain of the innexin ShakB(L) (41), direct observation of recombinant innexin gap junction plaques and the purification of innexin channels have not yet been reported. Here we established the overexpression and purification of *C. elegans* INX-6 gap junction channels using Sf9 cells and successfully obtained the class averages by single particle analysis.

The alkali extraction method is often used to isolate connexin gap junction plaques in native tissue and Sf9 cells (27, 30, 42, 43). In the present study, we used much milder conditions, such as a neutral pH and low ion concentration without reducing agents, to avoid INX-6 protein degeneration. Once solubilized in DDM, the oligomerized INX-6 channels were successfully purified with an affinity column using the similar protocol used for the purification of Cx26 (27). This may reflect the specific stability of INX-6 in the lipid bilayer and in detergent solution.

For more than three decades, a number of gap junction researchers have reported the structure of vertebrate gap junc-

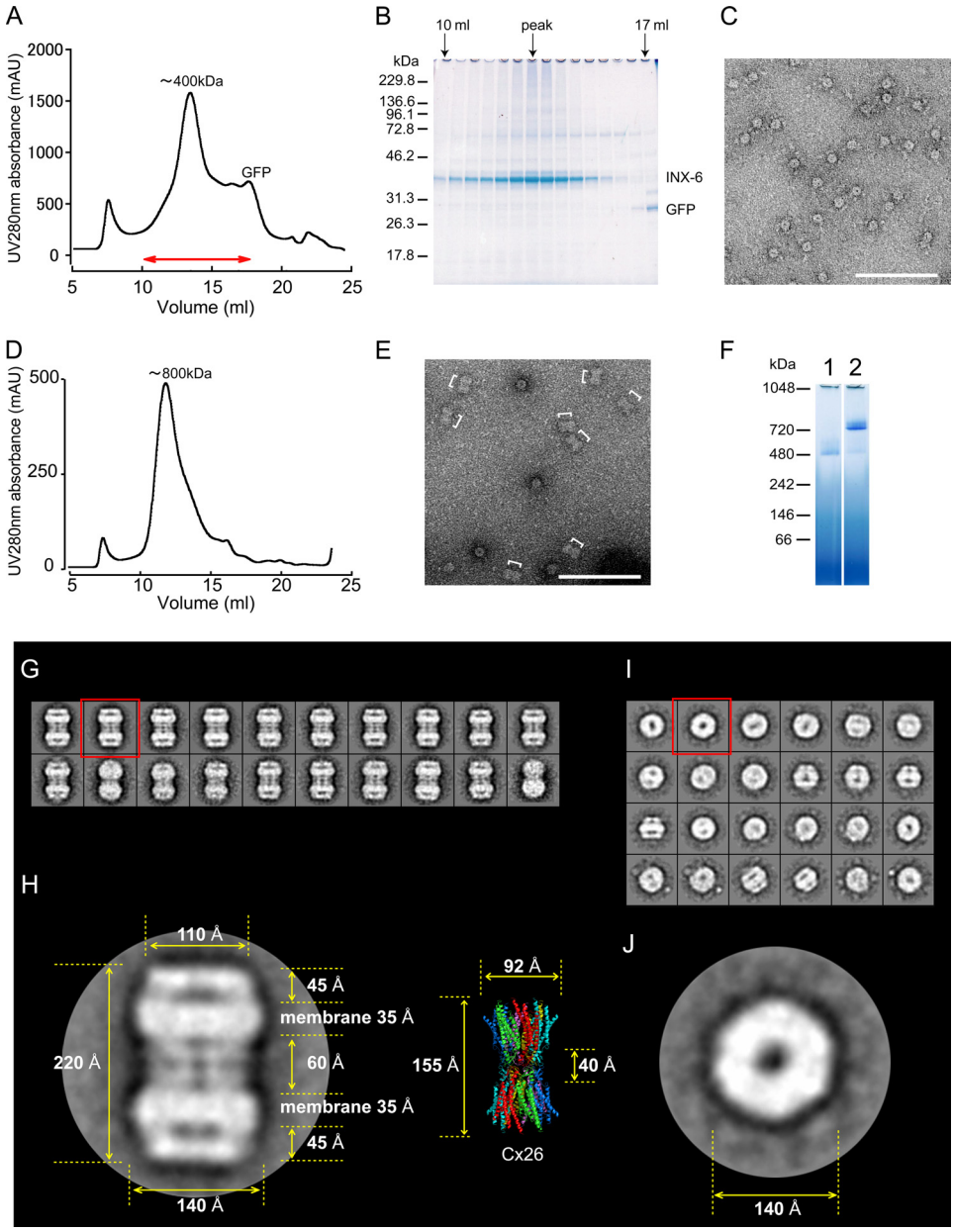

FIGURE 4. **EM and biochemical analysis of purified INX-6 channels.** *A*, diagram of size exclusion chromatography of INX-6 channels in 0.05% DDM buffer after removal of the GFP-His tag by thrombin. The highest peak appears at ~400 kDa. *mAU*, milliabsorbance units. *B*, SDS-PAGE analysis of eluted fractions recovered at the retention volume from 10 to 17 ml (marked by *red arrow* in *A*). This confirms that the highest peak in *A* corresponds to INX-6 peptides. *C*, negative stain image of the peak fraction at ~400 kDa in *A*. Some particles show the orientation with their pores perpendicular. *Bar* = 100 nm. *D*, elution diagram of purified INX-6 channels in 0.1% OGNG buffer gives rise to a peak at ~800 kDa. *E*, negative stain image of purified INX-6 channels sampled from the peak fraction at ~800 kDa in *C*. Double-barreled particles are marked by *square brackets*. *Bar* = 100 nm. *F*, native PAGE analysis of INX-6 channels shows main protein bands at ~480 kDa for INX-6/DDM (*lane 1*) and over 720 kDa for INX-6/OGNG (*lane 2*), consistent with the chromatographs (*A* and *D*). *G*, class averages of the particles picked from the ~800-kDa fraction in OGNG clearly demonstrate the side view of the docked junction form of INX-6. *H*, *left*, representative class average generated from 216 particles in the ~800-kDa fraction (indicated by *red square* in *G*) shows the docked junction form from the side view. Two detergent belts ~35 Å in width, corresponding to the transmembrane region, are clearly seen because stain cannot access this area. Because fewer detergent micelles are involved in the cytoplasmic ends, the width of 110 Å may be close to the actual size of the channel diameter. *Right*, ribbon model of Cx26 (20) for comparison. The scales for these two structures are adjusted. *I*, class averages picked from the ~400-kDa fraction exhibit various orientations with identical diameters. *J*, magnified representative of class average indicated by *red square* in *I* shows a top view of channels. 282 particles were combined for this average.

tions, comprising connexin, using isolated gap junction plaques or crystallized membrane sheets in a two-dimensional array (31–39). They usually form a hexagonal lattice in which the cell parameters range from 75 to 95 Å. This would be reasonable given that Cx26 is a dodecameric channel with a maximum channel diameter of 92 Å at the flexible cytoplasmic end (20). The hexagonal lattice of INX-6 gap junction plaques is similar to that of connexin (Fig. 3, *A* and *D*). The top view of the class average picked from the ~400-kDa fraction resembles a hexameric hemichannel (Fig. 4, *I* and *J*). However, the 1.2–1.5-fold difference in size of INX-6 and Cx26 would result in a 1.7–3.4-fold difference in volume. Even pentameric channels can form a hexagon-like lattice in two dimensions (44, 45). The oligomeric number of INX-6 must be carefully determined before performing structural studies using cryo-EM.

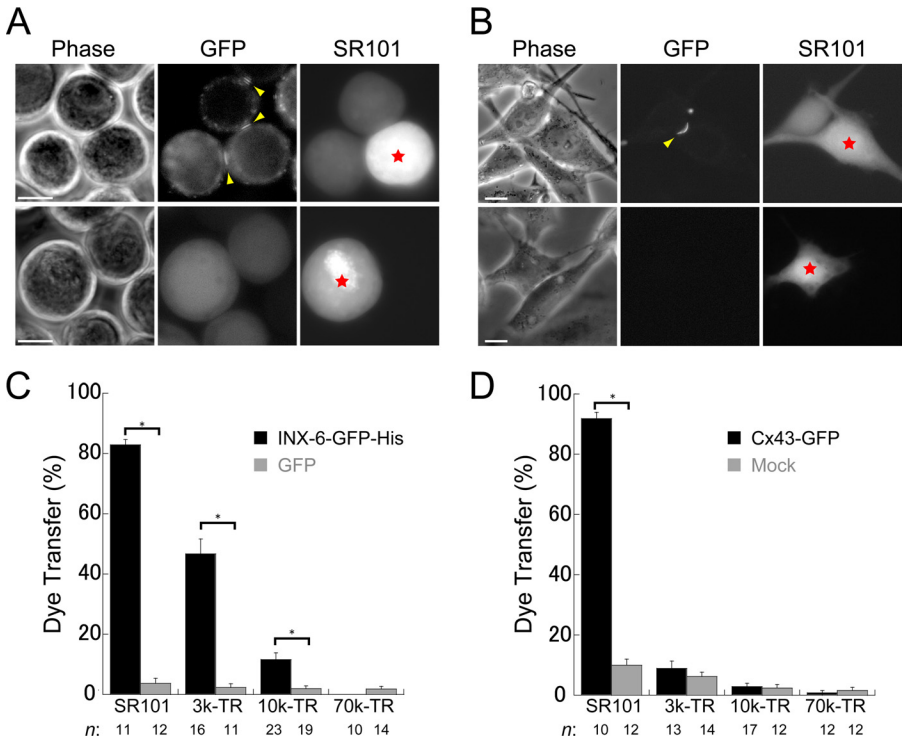

FIGURE 5. **Dye transfer analysis for INX-6-GFP-His and Cx43-GFP channels.** *A* and *B*, fluorescent images of SR101 (*SR*) microinjected cells denote the immediate dye transfer through INX-6-GFP-His and Cx43-GFP junctions. Phase contrast images (*left*), fluorescent images for GFP (*middle*), and fluorescent images for SR101 (*right*) are shown. *A*, Sf9 cells infected by recombinant INX-6-GFP-His viruses (*upper*) and recombinant GFP viruses (*lower*, control). *B*, HeLa cells after the induction of Cx43-GFP expression using 1 μg/ml doxycycline and 4.5 μM trichostatin A (*upper*) and without induction (*lower*). GFP signals corresponding to gap junction plaques are indicated by *yellow arrowheads*. Dye-injected cells are indicated by the *red stars*. All images were obtained 1 min after injection. *Bar* = 10 μm. *C* and *D*, statistical analyses of fluorescent dye transfer through INX-6-GFP-His and Cx43-GFP channels. Dye transfer proportion was statistically analyzed with four fluorescent tracers having a variety of sizes, 607-Da SR101, 3-kDa dextran-Texas Red (3K-TR), 10-kDa dextran-Texas Red (10K-TR), and 70-kDa dextran-Texas Red (70K-TR). Dye transfer was measured 1 min after injection. Assessed data for INX-6-GFP-His (*A*) and Cx43-GFP (*B*) are shown in *filled black columns*. Controls are indicated by *gray columns*. INX-6-GFP-His channels are more permeable to larger tracers such as 3K-TR and 10K-TR than Cx43-GFP channels. The numbers of injection sets are shown underneath as *n*. *Error bars* indicate standard errors. *, $p < 0.001$. All *p* values are based on Student's *t* test.

In early studies of the gap junction ultrastructure, crayfish gap junctions, probably comprising innexins, were determined by thin-section and negative stain EM to be ~170 Å in height with a unit cell of ~200 Å (22). The recent x-ray structure reveals that the height of Cx26 channels is about 155 Å with partially disordered cytoplasmic domains (20) (PDB code: 2ZW3). It is not straightforward to associate the crystal structure with thin-section EM observations due to artifacts produced during fixation or staining of the sample. The general consensus, however, with some exceptions (46), is that gap junctions from invertebrates have a larger junction membrane width, extracellular gap region, and channel diameter as compared with those from vertebrates (22, 23, 33, 47–53). Our measurements of INX-6 based on the class averages are consistent with these previous studies. Two-dimensional image averaging revealed that the purified vertebrate innexin homologs pannexin1 and pannexin2 channels have larger oligomer and pore diameters than Cx26 (54). The channel diameter for INX-6 is closer to that of pannexin1 than of Cx26 (140 Å for INX-6 and 120–160 Å for pannexin1, including detergent micelles). Although other innexin isoforms must be investigated for generalization of this trend, it is possible that the junction membrane width and molecular dimensions of innexins differ from those of connexins, due in part to the longer sequences of the extracellular loops of innexins.

The permeability of gap junction channels was previously estimated using fluorescent probes with various sizes and properties such as charge and shape, which established a molecular size cut-off of ~1 kDa for vertebrate gap junctions and ~2 kDa for invertebrate gap junctions (55, 56). Another study using fluorescent molecules conjugated with oligosaccharides, neutral branched glycopeptides, and charged linear peptides showed the transfer of molecules up to ~3 kDa (26). It is therefore not surprising that the 3k-TR tracer passed through the INX-6 channels in this study. The low but significant transfer of 10k-TR, with a dextran distribution range between 9000 and 11,000 Da, was however, contrary to our expectations (Fig. 5*C*). The permeability limits of pores would depend on substrate shape rather than molecular mass. Conjugated dextran is thought to have an elongated polysaccharide structure. Although linear peptides as large as 1.8 kDa effectively permeate Cx43 channels, circular 8-mer peptides do not (57). In fact, fluorescent dye-conjugated aprotinin, which has a molecular mass of ~6.5 kDa, did not pass through INX-6 channels (data not shown), probably because of the highly folded molecular structure with an α-helix and β-sheet that are larger than the pore diameter. Our results indicate that the INX-6 channel pore is more permeable than Cx43 and would probably be more permeable than most connexins as Cx43 is considered to have one of the largest limiting pore diameters in the connexin fam-

ily (40) with some exceptions for positively charged molecules (58). It remains unclear why gap junction channels with greater permeability predominate in invertebrates. The electrical synapse is common in invertebrates, and high permeability might be advantageous for simple and fast transmission. Because of the demand for complex communication, vertebrates may have developed unique coupling systems with distinct permeability, such as connexin.

Endogenous gap junction channels in Sf9 cells were inferred by electrophysiology (59). In all of our microinjection experiments, however, no high background activity was observed (Fig. 5). We cannot rule out some expression of endogenous innexin in Sf9 cells because *Sf-inx2*, which is close to *Drosophila inx-2*, has been identified (12). The expression of endogenous gap junction channels in Sf9 cells might not be high enough to affect the dye transfer background in our study. Alternatively, the electrical conductance of insect gap junction channels might not correlate with pore size. For connexin channels, there is likely no direct relation between channel conductance and ionic selectivity or dye permeability (60), which is supported by other studies (61, 62).

We successfully established the overexpression and purification of recombinant *C. elegans* INX-6 gap junction channels. Studies of the purified INX-6 gap junction channels revealed that they form a loosely packed hexagonal gap junction plaque that is similar to but distinct from connexins. The purified INX-6 channels, predominantly hemichannels in DDM and junction channels in OGNG, can be used for structural studies using high-resolution analysis. The class averages of purified INX-6 channels revealed that the molecular dimensions of the junction form of INX-6 are greater than those of Cx26. Future cryo-EM studies could elucidate the oligomeric number of INX-6 channels, which remains unclear in the present study. Dye transfer assays revealed that INX-6 channels have higher permeability than Cx43-GFP channels. Our findings provide insight into the morphology and characteristic permeability of recombinant innexin channels. The biologic significance of INX-6 pores with higher permeability remains to be determined. Further structural and functional studies of innexin channels will enhance our understanding of the mysteriously fast gating channels observed in crayfish, such as those that can close within 1.0 ms (63, 64).

Acknowledgments—The C. elegans cDNA library was kindly provided by Dr. Sakiko Honjoh (Kyoto University). We are grateful to Kanako Hoshino (Kyoto University) for INX-6 expression and Sf9 cell culture. We also thank Dr. Kazutoshi Tani (Nagoya University) for assistance with the image processing for the single particle analysis.

REFERENCES

1. Loewenstein, W. R. (1981) Junctional intercellular communication: the cell-to-cell membrane channel. *Physiol. Rev.* **61,** 829–913
2. Dbouk, H. A., Mroue, R. M., El-Sabban, M. E., and Talhouk, R. S. (2009) Connexins: a myriad of functions extending beyond assembly of gap junction channels. *Cell Commun. Signal.* **7,** 4
3. Bennett, M. V., and Zukin, R. S. (2004) Electrical coupling and neuronal synchronization in the Mammalian brain. *Neuron* **41,** 495–511
4. Baker T. S., Caspar D. L., Hollingshead C. J., and Goodenough D. A. (1983) Gap junction structures. IV. Asymmetric features revealed by low-irradiation microscopy. *J. Cell Biol.* **96,** 204–216
5. Kumar N. M., and Gilula N. B. (1996) The gap junction communication channel. *Cell* **84,** 381–388
6. Phelan, P., and Starich T. A. (2001) Innexins get into the gap. *Bioessays* **23,** 388–396
7. Phelan P., Bacon J. P., Davies J. A., Stebbings L. A., Todman M. G., Avery L., Baines R. A., Barnes T. M., Ford C., Hekimi S., Lee R., Shaw J. E., Starich T. A., Curtin K. D., Sun Y. A., and Wyman R. J. (1998) Innexins: a family of invertebrate gap-junction proteins. *Trends Genet.* **14,** 348–349
8. Starich, T. A., Herman, R. K., and Shaw J. E. (1993) Molecular and genetic analysis of unc-7, a *Caenorhabditis elegans* gene required for coordinated locomotion. *Genetics* **133,** 527–541
9. Starich, T. A., Lee, R. Y., Panzarella, C., Avery, L., and Shaw, J. E. (1996) eat-5 and unc-7 represent a multigene family in *Caenorhabditis elegans* involved in cell-cell coupling. *J. Cell Biol.* **134,** 537–548
10. Phelan, P., Nakagawa, M., Wilkin, M. B., Moffat, K. G., O'Kane, C. J., Davies, J. A., and Bacon, J. P. (1996) Mutations in shaking-B prevent electrical synapse formation in the *Drosophila* giant fiber system. *J. Neurosci.* **16,** 1101–1113
11. Phelan P., Stebbings L. A., Baines R. A., Bacon J. P., Davies J. A., and Ford C. (1998) *Drosophila* Shaking-B protein forms gap junctions in paired *Xenopus* oocytes. *Nature* **391,** 181–184
12. Phelan, P. (2005) Innexins: members of an evolutionarily conserved family of gap-junction proteins. *Biochim. Biophys. Acta.* **1711,** 225–245
13. Kandarian, B., Sethi, J., Wu, A., Baker, M., Yazdani, N., Kym, E., Sanchez, A., Edsall, L., Gaasterland, T., and Macagno, E. (2012) The medicinal leech genome encodes 21 innexin genes: different combinations are expressed by identified central neurons. *Dev. Genes Evol.* **222,** 29–44
14. Panchin Y., Kelmanson I., Matz M., Lukyanov K., Usman N., and Lukyanov S. (2000) A ubiquitous family of putative gap junction molecules. *Curr. Biol.* **10,** R473-R474
15. Woehrle T, Yip L, Manohar M, Sumi Y, Yao Y, Chen Y, and Junger WG. (2010) Hypertonic stress regulates T cell function via pannexin-1 hemichannels and P2X receptors. *J. Leukoc. Biol.* **88,** 1181–1189
16. Chekeni F. B., Elliott M. R., Sandilos J. K., Walk S. F., Kinchen J. M., Lazarowski E. R., Armstrong A. J., Penuela S., Laird D. W., Salvesen G. S., Isakson B. E., Bayliss D. A., and Ravichandran K. S. (2010) Pannexin 1 channels mediate 'find-me' signal release and membrane permeability during apoptosis. *Nature.* **467,** 863–867
17. Altun, Z. F., Chen, B., Wang, Z. W., and Hall, D. H. (2009) High resolution map of *Caenorhabditis elegans* gap junction proteins. *Dev. Dyn.* **238,** 1936–1950
18. Li, S., Dent, J. A., and Roy, R. (2003) Regulation of intermuscular electrical coupling by the *Caenorhabditis elegans* innexin inx-6. *Mol. Biol. Cell.* **14,** 2630–2644
19. Oshima, A., Tani, K., Hiroaki, Y., Fujiyoshi, Y., and Sosinsky, G. E. (2007) Three-dimensional structure of a human connexin26 gap junction channel reveals a plug in the vestibule. *Proc. Natl. Acad. Sci. U.S.A.* **104,** 10034–10039
20. Maeda, S., Nakagawa, S., Suga, M., Yamashita, E., Oshima, A., Fujiyoshi, Y., and Tsukihara, T. (2009) Structure of the connexin 26 gap junction channel at 3.5 A resolution. *Nature* **458,** 597–602
21. Oshima, A., Tani, K., Toloue, M. M., Hiroaki, Y., Smock, A., Inukai, S., Cone, A., Nicholson, B. J., Sosinsky, G. E., and Fujiyoshi, Y. (2011) Asymmetric configurations and N-terminal rearrangements in connexin26 gap junction channels. *J. Mol. Biol.* **405,** 724–735
22. Peracchia, C. (1973) Low resistance junctions in crayfish. II. Two arrays of globules in junctional membranes. *J. Cell Biol.* **57,** 66–76
23. Ohta Y., Nishikawa K., Hiroaki Y., and Fujiyoshi Y. (2011) Electron tomographic analysis of gap junctions in lateral giant fibers of crayfish. *J. Struct. Biol.* **175,** 49–61
24. Whitten S. J., and Miller M. A. (2007) The role of gap junctions in *Caenorhabditis elegans* oocyte maturation and fertilization. *Dev. Biol.* **301,** 432–446
25. Yeh E., Kawano T., Ng S., Fetter R., Hung W., Wang Y., and Zhen M. (2009) *Caenorhabditis elegans* innexins regulate active zone differentiation. *J. Neurosci.* **29,** 5207–5217
26. Schwarzmann, G., Wiegandt, H., Rose, B., Zimmerman, A., Ben-Haim, D.,

and Loewenstein, W. R. (1981) Diameter of the cell-to-cell junctional membrane channels as probed with neutral molecules. *Science* **213,** 551–553
27. Oshima, A., Doi, T., Mitsuoka, K., Maeda, S., and Fujiyoshi, Y. (2003) Roles of Met-34, Cys-64, and Arg-75 in the assembly of human connexin 26: implication for key amino acid residues for channel formation and function. *J. Biol. Chem.* **278,** 1807–1816
28. Unger, V. M., Kumar, N. M., Gilula, N. B., and Yeager, M. (1997) Projection structure of a gap junction membrane channel at 7 Ä resolution. *Nat. Struct. Biol.* **4,** 39 – 43
29. Ludtke, S. J., Baldwin, P. R., and Chiu, W. (1999) EMAN: semiautomated software for high-resolution single-particle reconstructions. *J. Struct. Biol.* **128,** 82–97
30. Stauffer, K. A., Kumar, N. M., Gilula, N. B., and Unwin, N. (1991) Isolation and purification of gap junction channels. *J. Cell Biol.* **115,** 141–150
31. Makowski, L., Caspar, D. L., Phillips, W. C., and Goodenough, D. A. (1977) Gap junction structures. II. Analysis of the x-ray diffraction data. *J. Cell Biol.* **74,** 629 – 645
32. Zampighi, G., and Unwin, P. N. (1979) Two forms of isolated gap junctions. *J. Mol. Biol.* **135,** 451– 464
33. Unwin, P. N., Ennis, P. D. (1984) Two configurations of a channel-forming membrane protein. *Nature.* **307,** 609 – 613
34. Lampe, P. D., Kistler, J., Hefti, A., Bond, J., Müller, S., Johnson, R. G., and Engel, A. (1991) *In vitro* assembly of gap junctions. *J. Struct. Biol.* **107,** 281–290
35. Yeager, M., and Gilula, N. B. (1992) Membrane topology and quaternary structure of cardiac gap junction ion channels. *J. Mol. Biol.* **223,** 929 –948
36. Kistler, J., Bond, J., Donaldson, P., and Engel, A. (1993) Two distinct levels of gap junction assembly in vitro. *J. Struct. Biol.* **110,** 28 –38
37. Unger, V. M., Kumar, N. M., Gilula, N. B., and Yeager, M. (1999) Three-dimensional structure of a recombinant gap junction membrane channel. *Science.* **283,** 1176 –1180
38. Hand, G. M., Müller, D. J., Nicholson, B. J., Engel, A., and Sosinsky, G. E. (2002) Isolation and characterization of gap junctions from tissue culture cells. *J. Mol. Biol.* **315,** 587– 600
39. Cheng, A., Schweissinger, D., Dawood, F., Kumar, N., and Yeager, M. (2003) Projection structure of full length connexin 43 by electron cryocrystallography. *Cell Commun. Adhes.* **10,** 187–191
40. Harris, A. L. (2001) Emerging issues of connexin channels: biophysics fills the gap. *Q. Rev. Biophys.* **34,** 325– 472
41. Depriest, A., Phelan, P., and Skerrett, M. I. (2011) Tryptophan scanning mutagenesis of the first transmembrane domain of the innexin Shaking-B(Lethal). *Biophys. J.* **101,** 2408 –2416
42. Hertzberg, E. L. (1984) A detergent-independent procedure for the isolation of gap junctions from rat liver. *J. Biol. Chem.* **259,** 9936 –9943
43. Stauffer, K. A. (1995) The gap junction proteins β1-connexin (connexin-32) and β2-connexin (connexin-26) can form heteromeric hemichannels. *J. Biol. Chem.* **270,** 6768 – 6872
44. Saint, N., Lacapère, J. J., Gu, L. Q., Ghazi, A., Martinac, B., and Rigaud, J. L. (1998) A hexameric transmembrane pore revealed by two-dimensional crystallization of the large mechanosensitive ion channel (MscL) of *Escherichia coli*. *J. Biol. Chem.* **273,** 14667–14670
45. Chang, G., Spencer, R. H., Lee, A. T., Barclay, M. T., and Rees, D. C. (1998) Structure of the MscL homolog from *Mycobacterium tuberculosis*: a gated mechanosensitive ion channel. *Science.* **282,** 2220 –2226
46. Yeager, M. (1998) Structure of cardiac gap junction intercellular channels. *J. Struct. Biol.* **121,** 231–245
47. Peracchia, C. (1973) Low resistance junctions in crayfish. I. Structural details and further evidence for intercellular channels by freeze-fracture and negative staining. *J. Cell Biol.* **57,** 54 – 65
48. Gilula, N. B. (1978) in *Intercellular Junctions and Synapses* (Feldman, J., Gilula, N. B., and Pitts, J. D., eds), pp. 1–22, Chapman and Hall, London
49. Zampighi, G., Ramón, F., and Durán, W. (1978) Fine structure of the electrotonic synapse of the lateral giant axons in a crayfish (*Procambarus clarkii*). *Tissue Cell* **10,** 413– 426
50. Berdan, R. C., and Gilula, N. B. (1988) The arthropod gap junction and pseudo-gap junction: isolation and preliminary biochemical analysis. *Cell Tissue Res.* **251,** 257–274
51. Zampighi, G., Kreman, M., Ramón, F., Moreno, A. L., and Simon, S. A. (1988) Structural characteristics of gap junctions. I. Channel number in coupled and uncoupled conditions. *J. Cell Biol.* **106,** 1667–1678
52. Bosch, E. (1989) Comparative study of neuronal and glial gap-junctions in crayfish nerve cords. *J. Comp. Neurol.* **285,** 399 – 411
53. Hirokawa, N., and Heuser, J. (1982) The inside and outside of gap-junction membranes visualized by deep etching. *Cell.* **30,** 395– 406
54. Ambrosi, C., Gassmann, O., Pranskevich, J. N., Boassa, D., Smock, A., Wang, J., Dahl, G., Steinem, C., and Sosinsky, G. E. (2010) Pannexin1 and Pannexin2 channels show quaternary similarities to connexons and different oligomerization numbers from each other. *J. Biol. Chem.* **285,** 24420 –24431
55. Simpson, I., Rose, B., and Loewenstein, W. R. (1977) Size limit of molecules permeating the junctional membrane channels. *Science* **195,** 294 –296
56. Flagg-Newton, J., and Loewenstein, W. R. (1979) Experimental depression of junctional membrane permeability in mammalian cell culture. A study with tracer molecules in the 300 to 800 Dalton range. *J. Membr. Biol.* **50,** 65–100
57. Neijssen, J., Herberts, C., Drijfhout, J. W., Reits, E., Janssen, L., and Neefjes, J. (2005) Cross-presentation by intercellular peptide transfer through gap junctions. *Nature* **434,** 83– 88
58. Kanaporis, G., Brink, P. R., and Valiunas, V. (2011) Gap junction permeability: selectivity for anionic and cationic probes. *Am. J. Physiol. Cell Physiol.* **300,** C600 –C609
59. Bukauskas, F. F., Vogel, R., and Weingart, R. (1997) Biophysical properties of heterotypic gap junctions newly formed between two types of insect cells. *J. Physiol.* **499,** 701–713
60. Veenstra, R. D., Wang, H. Z., Beblo, D. A., Chilton, M. G., Harris, A. L., Beyer, E. C., and Brink, P. R. (1995) Selectivity of connexin-specific gap junctions does not correlate with channel conductance. *Circ. Res.* **77,** 1156 –1165
61. Bukauskas F. F., Elfgang C., Willecke K., and Weingart R. (1995) Heterotypic gap junction channels (connexin26 - connexin32) violate the paradigm of unitary conductance. *Pflügers Arch.* **429,** 870 – 872
62. Suchyna, T. M., Nitsche, J. M., Chilton, M., Harris, A. L., Veenstra, R. D., and Nicholson B. J. (1999) Different ionic permeabilities for connexins 26 and 32 produce rectifying gap junction channels. *Biophys. J.* **77,** 2968 –2987
63. Furshpan, E. J., and Potter, D. D. (1959) Transmission at the giant motor synapses of the crayfish. *J. Physiol.* **145,** 289 –325
64. Giaume, C., Kado, R. T., and Korn, H. (1987) Voltage-clamp analysis of a crayfish rectifying synapse. *J. Physiol.* **386,** 91–112